CHEMISTRY OF MATERIALS
Cite This: Chem. Mater. 2019, 31, 6424−6434
Review
pubs.acs.org/cm

Superexchange Induced Charge Transport in Organic Donor−Acceptor Cocrystals and Copolymers: A Theoretical Perspective

Hua Geng,[†,‡] Lingyun Zhu,[∥] Yuanping Yi,*[,‡] Daoben Zhu,[‡] and Zhigang Shuai*[,§,‡]

[†]Department of Chemistry, Beijing Advanced Innovation Center for Imaging Theory and Technology, Capital Normal University, Beijing 100048, China

[‡]Beijing National Laboratory for Molecular Sciences, CAS Key Laboratory of Organic Solids, Institute of Chemistry, Chinese Academy of Sciences, Beijing 100190, China

[§]MOE Key Laboratory of Organic OptoElectronics and Molecular Engineering, Department of Chemistry, Tsinghua University, Beijing 100084, China

[∥]CAS Key Laboratory of Nanosystem and Hierarchical Fabrication, CAS Center for Excellence in Nanoscience, National Center for Nanoscience and Technology, Beijing 100190, China

ABSTRACT: Organic donor−acceptor (D−A) blending systems have displayed great potential in the application of organic optoelectronics. Conventionally, charge transport is not allowed along the stacking direction for D−A mixed-stack organic cocrystals or along the intrachain backbone direction for D−A copolymers, since the nearest-neighbored D or A molecules/units are too far away to interact directly with each other. In fact, for hole (electron) transport, an effective electronic coupling between adjacent D (A) molecules/units can be manifested by a superexchange mechanism with the in between A (D) molecule/unit as a bridge. In this perspective, we have briefly summarized our recent progress in understanding the long-range superexchange electronic couplings to assess the charge transport and polarities of D−A cocrystals and copolymers. The energy-splitting and partition-based methods are first introduced to evaluate the bridge-mediated superexchange couplings. The important role of the superexchange mechanism in the charge transport is then discussed, and the similarity and difference between D−A cocrystals and copolymers are elucidated. Finally, the factors that determine the charge carrier polarities and the magnitudes of superexchange couplings are analyzed to provide some insightful principles for the design of high-mobility organic semiconductors based on D−A blending systems.

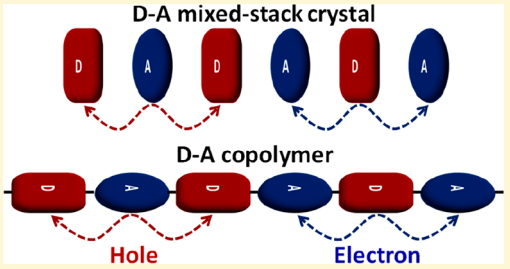

1. INTRODUCTION

Multicomponent organic semiconductors have demonstrated great potential in the applications of organic optoelectronic devices, such as organic field effect transistors (OFETs) and organic light-emitting diodes (OLEDs).[1−6] The donor−acceptor (D−A) mixed-stack cocrystals, usually considered as insulators previously, have proved to have remarkable ambipolar transport properties from both experimental and theoretical investigations in recent years.[7−12] However, traditionally, in these molecular blending or cocrystal systems, the charge carriers transport along the main material and the dopants act as carrier traps, which is detrimental to charge transport. To address this issue, a long-range superexchange mechanism was proposed to play an essential role in the charge transport for such D−A cocrystals and different charge transport properties were predicted by theoretical calculations.[7,13,14] Since then, an increasing number of organic D−A mixed-stack crystals have been reported by different experimental groups and displayed good ambipolar or electron-/hole-dominant charge transport properties.[15−33]

On the other hand, high charge mobilities have also been observed in various D−A copolymers.[34−37] For instance, Heeger et al. reported a hole mobility even exceeding 50 $cm^2/(V\ s)$ for the OFET devices based on cyclopentadithiophene-pyridinethiadiazole (CDT−PT),[38] which represents the highest mobility for polymeric semiconductors. Through combining different donor and acceptor units for the copolymerization, the charge mobilities could be modulated in a wide range from 10^{-2} to dozens of $cm^2/(V\ s)$.[39−41] Notably, the diketopyrrolopyrrole (DPP)-based copolymers were found to exhibit diversified transport polarities.[42−44] In contrast, the underlying charge transport mechanisms in the D−A copolymers remain under debate. Fornari and Troisi suggest that the hopping barrier between the mobility edge and carrier energy level can be reduced by a narrower bandwidth.[45] We argued that the bandwidth originates from a synergistic effect of static disorder (or site energy distribution) and direct electronic coupling between the D and A units; the former is destructive, but the latter is constructive to charge transport. Thus, it is difficult to judge the charge transport properties

Special Issue: Jean-Luc Bredas Festschrift

Received: April 18, 2019
Revised: June 18, 2019
Published: July 11, 2019

DOI: 10.1021/acs.chemmater.9b01545
Chem. Mater. 2019, 31, 6424−6434

from bandwidths only. From the perspective of long-range superexchange, we have demonstrated that the D−A copolymers can intrinsically possess ultrasmall effective charge carrier masses and provided the rationalization of ultrahigh charge mobilities and various transport polarities.[46,47]

In this perspective, we first introduce the theoretical methodologies for evaluation of the superexchange couplings for D−A cocrystals and copolymers and summarize the similarity and difference of superexchange charge transport between D−A cocrystals and copolymers. Then, the influence factors to determine the carrier polarities and the magnitudes of superexchange couplings are discussed with the aim to elucidate the design principles to obtain high-mobility organic semiconductors with desired charge carrier polarities.

2. THEORETICAL METHODOLOGIES

Compared with single-component materials, the properties of multicomponent materials are much more complex. Taking the DMQtT−F4TCNQ (DMQtT = dimethylquaterthiophene, F4TCNQ = 2,3,5,6-tetrafluoro-7,7,8,8-tetracyano-quinodimethane) system as a representative of D−A cocrystals (see Scheme 1a),[48] the donor molecule of DMQtT interacts with the acceptor molecule of F4TCNQ through weak intermolecular interaction, such as van der Waals and electrostatic interactions. For the representative 2T−BT (2T = bithiophene, BT = benzothiadiazole) system of D−A copolymers, while the donor of 2T and acceptor of BT units are linked by relatively strong covalent bonds, the D and A components are characteristic of significant localized molecular orbitals and the molecular orbitals of the entire copolymer chain can be physically regarded as a linear combination of the fragmental molecular orbitals of 2T and BT. Upon cocrystallization or copolymerization of the donor and acceptor moieties, the donor (acceptor) fragments are separated by the acceptor (donor) fragments and they are not directly coupled electronically. The effective coupling between adjacent donors (acceptors) is mediated by the middle acceptor (donor), i.e., via the superexchange mechanism (Scheme 1b).

Scheme 1. Illustration of the Structures of the DMQtT−F_4TCNQ Cocrystal and 2T−PT Copolymer (a) and the Superexchange Mechanism for Hole and Electron Transport in D−A Cocrystals and Copolymers (b)

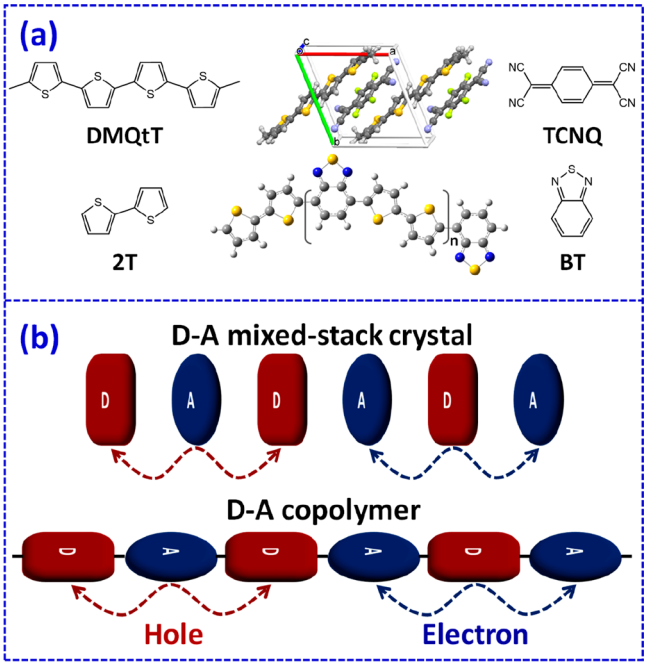

To illustrate the effect of the superexchange interaction on the band structures, we recall the one-dimensional tight-binding model that consists of two different types of sites (e.g., D and A) in each repeat unit. For simplicity, here only the HOMO (LUMO) of D and A is considered in the hole (electron) transport, and the one-dimensional tight-binding model Hamiltonian can be written as follows

$$H = V_{DA}\sum_i (|D_i\rangle\langle A_i| + |A_i\rangle\langle D_{i+1}| + \text{h.c.}) + \varepsilon_D\sum_i (|D_i\rangle\langle D_i|) + \varepsilon_A\sum_i (|A_i\rangle\langle A_i|) \quad (1)$$

where ε_D, ε_A, and ε_{DA} represent the D and A site energies and the electronic coupling between adjacent D and A, respectively. In our cases, the distance between adjacent D and A is one-half of the size of the unit cell (a). After discrete Fourier transform, the Hamiltonian matrix can be expressed in the k space as follows:

$$\mathcal{H}(k) = \begin{vmatrix} \varepsilon_D & -2V_{DA}\cos(ka/2) \\ -2V_{DA}\cos(ka/2) & \varepsilon_A \end{vmatrix} \quad (2)$$

Then, we can obtain the energy dispersion relation by diagonalizing the above matrix

$$E(k) = \frac{\varepsilon_D + \varepsilon_A}{2} \pm \sqrt{\left(\frac{\varepsilon_D - \varepsilon_A}{2}\right)^2 + \left[2V_{DA}\cos\left(\frac{ka}{2}\right)\right]^2} \quad (3)$$

From the above band dispersion, the bandwidth and effective mass can be derived for various site energy differences between D and A ($\Delta\varepsilon = \varepsilon_D - \varepsilon_A$):

$$w = \begin{cases} 4V_{DA} & \Delta\varepsilon = 0 \\ \sqrt{(\Delta\varepsilon/2)^2 + 4V_{DA}{}^2} - \Delta\varepsilon/2 & = \begin{cases} 2V_{DA} & 0 < \Delta\varepsilon \ll V_{DA} \\ 4V^{\text{eff}} & \Delta\varepsilon \gg V_{DA} \end{cases} \end{cases} \quad (4)$$

$$m^* = -\frac{\hbar^2}{a^2 V_{DA}{}^2}\sqrt{(\Delta\varepsilon/2)^2 + 4V_{DA}{}^2} = \begin{cases} -\dfrac{\hbar^2}{2(a/2)^2 V_{DA}} & \Delta\varepsilon \ll V_{DA} \\ -\dfrac{\hbar^2}{2a^2 V^{\text{eff}}} & \Delta\varepsilon \gg V_{DA} \end{cases} \quad (5)$$

Here, $V^{\text{eff}} = V_{DA}{}^2/\Delta\varepsilon$ is the superexchange coupling and $\hbar$ is the Planck constant. It can be seen that in contrast to the homopolymers or single-component molecular crystals (i.e., $\Delta\varepsilon \ll V_{DA}$), in which the effective mass is determined by the direct coupling (V_{DA}) between adjacent D and A, the effective mass of the D−A copolymers or cocrystals (i.e., $\Delta\varepsilon \gg V_{DA}$) is defined by the superexchange coupling (V^{eff}).

As seen in Figure 1, in the case of a homopolymer with $\Delta\varepsilon$ = 0 eV and V_{DA} = 0.5 eV, the bandwidth is equal to 2 eV. When the site energy difference is introduced just like the mixed D−

DOI: 10.1021/acs.chemmater.9b01545
Chem. Mater. 2019, 31, 6424−6434

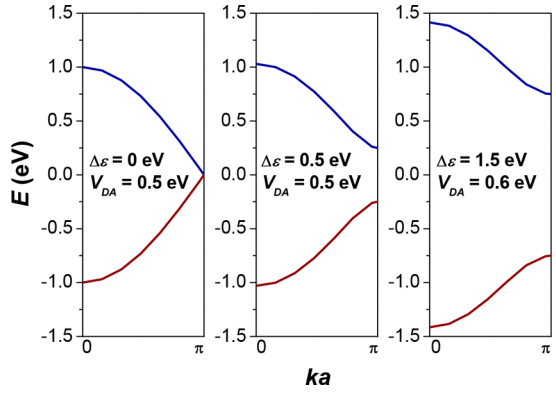

Figure 1. Band structures calculated by using the one-dimensional tight-binding model with different site energy difference ($\Delta\varepsilon$) and direct electronic coupling between donor and acceptor units (V_{DA}).

A case, the band structure will be splitted into two parts; when $\Delta\varepsilon$ is increased to be as large as V_{DA}, the bandwidth is much narrowed (0.78 eV), whereas the effective mass is hardly changed. In the case of a remarkably enlarged $\Delta\varepsilon$ (1.5 eV) and a slightly stronger V_{DA} (0.6 eV), although the bandwidth (0.67 eV) becomes much narrower than that of the homopolymer, the effective mass is smaller than that of the homopolymer. Therefore, the long-range superexchange couplings (effective coupling) can play an important role in the charge transport of the D−A cocrystals and copolymers. In the following, we will introduce two computational methods for evaluation of the superexchange couplings.

2.1. Energy Splitting Method. Energy splitting in the dimer method has been widely used to evaluate the electronic coupling between two adjacent molecules.[49,50] To account for the role of the mediate bridge, the superexchange electronic couplings should be derived on the basis of a bridge-mediated triad [(monomer 1)−bridge−(monomer 2)]. For the D−A cocrystals and copolymers, the superexchange coupling is calculated as the energy difference between the HOMO and HOMO−1 of the DAD triad for hole transport while as the energy difference between the LUMO+1 and LUMO of the ADA triad for electron transport (see Scheme 1b):

$$V_h^{eff} = (E_{HOMO}^{DAD} - E_{HOMO-1}^{DAD})/2 \quad (6)$$

$$V_e^{eff} = (E_{LUMO+1}^{ADA} - E_{LUMO}^{ADA})/2 \quad (7)$$

As shown in Figure 2, the calculated superexchange coupling in the DMQtT−F4TCNQ mixed-stack crystal is 102 and 97 meV for holes and electrons, respectively. As a consequence of the strong superexchange coupling, the effective mass along the stacking direction is estimated to be as small as 0.20 and 0.26 m_0 for holes and electrons, respectively; thus, the DMQtT−F4TCNQ mixed-stack crystal can exhibit remarkable ambipolar transport performance.[7] Recently, various organic D−A mixed-stack systems have been synthesized and found to display good charge transport properties, which could be reasonably explained by the energy-splitting calculated superexchange couplings.[8,12,16,17,21,24,33] For the D−A copolymers, the polarized energies of the HOMO and LUMO for the acceptor segments are all lower than those of the donor segments; thus, the energy level alignments present a staggered type and are similar to the D−A cocrystals. In the case of the 2T−BT copolymer, the triad system is chosen as BT−2T−BT for electrons and as 2T−BT−2T for holes. The calculated

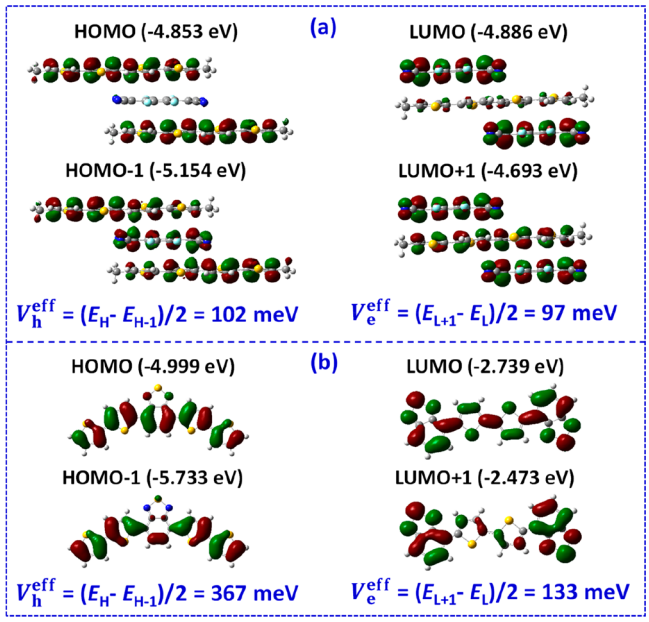

Figure 2. Energy-splitting estimates of the superexchange coupling holes and electrons (a) along the stacking direction in the DMQtT−F4TCNQ and (b) along the backbone direction for the 2T−BT copolymer (H, HOMO; L, LUMO).

superexchange coupling is as large as 367 and 133 meV for holes and electrons, respectively. Consequently, the effective mass along the backbone direction is extremely small, only 0.10 m_0 for holes and 0.22 m_0 for electrons.[47] When two monomers are not in equivalent positions in a dimer, the energy splitting estimated electronic coupling for the dimer has been demonstrated qualitatively incorrectly due to the polarization effect.[51] In the case of a DAD or ADA triad, the polarization effect can be even stronger; thus, the application of the energy splitting method would be more limited in two-component D−A cocrystals or copolymers.[14] Next, we will introduce a general method based on the Larsson partition technique to evaluate the superexchange coupling.

2.2. Larsson Partition Method. As described above, the superexchange coupling should be estimated on the basis of a (monomer 1)−bridge−(monomer 2) triad (DAD for holes and ADA for electrons; for D−A copolymers, the two ends of the triad are saturated by hydrogen atoms). The electronic properties of the triad system can be described by the following secular equation

$$HC = ESC \quad (8)$$

where H and S denote the system Hamiltonian and overlap matrices, respectively, and E and C are the orbital energies and wave functions of the triad system. For D−A copolymers, the orbitals of the entire copolymer chain should be clearly regarded as a linear combination of the localized orbitals of the decomposed donor and acceptor moieties that are saturated by hydrogen atoms. After projection to the localized orbitals on the two monomers 1 and 2 and the middle bridge, the H and S matrices can be expressed as

$$H = \begin{pmatrix} \varepsilon_1 & V_{12} & V_{1B} \\ V_{21} & \varepsilon_2 & V_{2B} \\ V_{B1} & V_{B2} & \varepsilon_B \end{pmatrix} \quad (9)$$

DOI: 10.1021/acs.chemmater.9b01545
Chem. Mater. 2019, 31, 6424−6434

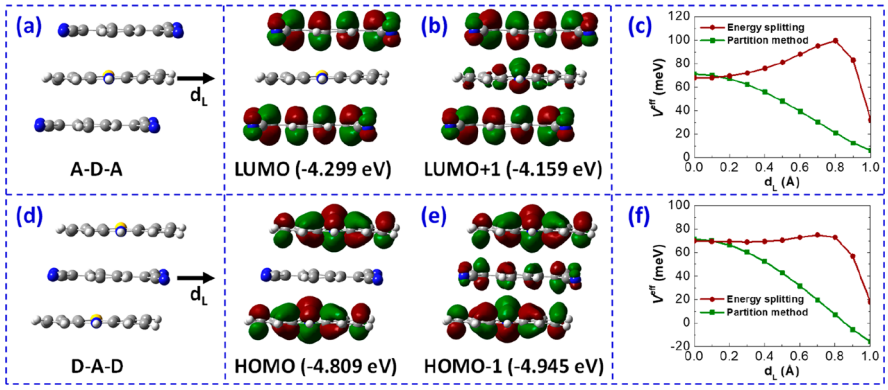

Figure 3. Dependence of the superexchange couplings along the stacking direction of the PTZ−TCNQ crystal calculated by the energy splitting and partition-based methods on the longitude displacement of the middle bridge.

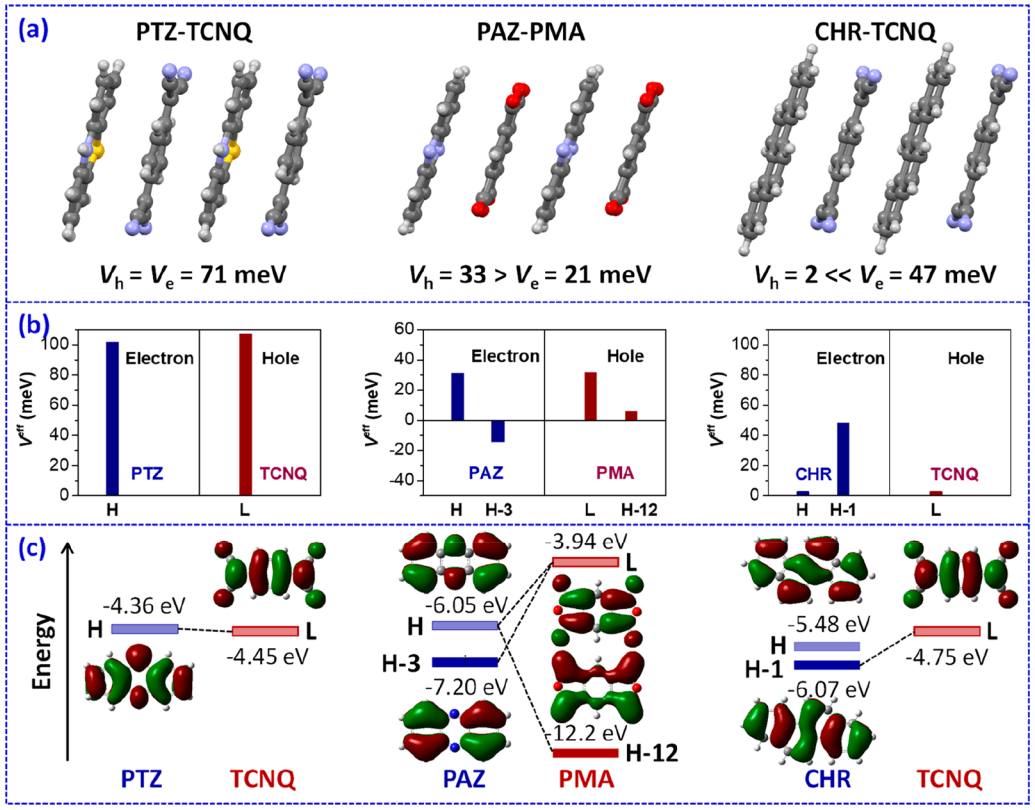

Figure 4. (a) Molecular stacking structures in the PTZ−TCNQ, PAZ−PMA, and CHR−TCNQ cocrystals; (b) contributions of essential bridge orbitals to the superexchange couplings; (c) important molecular orbitals of the donor and acceptor components involved in the superexchange interaction.

$$S = \begin{pmatrix} 1 & S_{12} & S_{1B} \\ S_{21} & 1 & S_{2B} \\ S_{B1} & S_{B2} & 1 \end{pmatrix} \tag{10}$$

The related matrix elements can be computed according to the following equations:

$$\varepsilon_i = \langle \psi_i | H | \psi_i \rangle \tag{11}$$

$$V_{ij} = V_{ji} = \langle \psi_i | H | \psi_j \rangle \tag{12}$$

$$S_{ij} = S_{ji} = \langle \psi_i | \psi_j \rangle \tag{13}$$

Here, ψ_i and ψ_j represent the molecular orbitals of the isolated monomers or bridge. For hole (electron) transport, ψ_1, ψ_2, and ψ_B are the HOMO (LUMO) of two donor (acceptor) monomers and the molecular orbitals of the middle acceptor (donor) bridge, respectively. After Löwdin's symmetric transformation, the Hamiltonian can be expressed by an orthogonalized basis[52]

$$\tilde{H} = S^{-1/2} H S^{-1/2} = \begin{pmatrix} \tilde{\varepsilon}_1 & \tilde{V}_{12} & \tilde{V}_{1B} \\ \tilde{V}_{21} & \tilde{\varepsilon}_2 & \tilde{V}_{2B} \\ \tilde{V}_{B1} & \tilde{V}_{B2} & \tilde{\varepsilon}_B \end{pmatrix} \tag{14}$$

DOI: 10.1021/acs.chemmater.9b01545
Chem. Mater. 2019, 31, 6424−6434

where $\tilde{V}_{1B}$, $\tilde{V}_{2B}$, $\tilde{V}_{B1}$, and $\tilde{V}_{B2}$ are vectors and $\tilde{\varepsilon}_B$ is a matrix. Like the site-energy overlap correction in the dimer, such basis orthogonalization can take the polarization effect into consideration. Then, the effective Hamiltonian matrix can be obtained by applying Larsson partition within the perturbation scheme:[53]

$$H^{\text{eff}} = \begin{pmatrix} \varepsilon_1^{\text{eff}} & V_{12}^{\text{eff}} \\ V_{21}^{\text{eff}} & \varepsilon_2^{\text{eff}} \end{pmatrix} = \begin{pmatrix} \tilde{\varepsilon}_1 & \tilde{V}_{12} \\ \tilde{V}_{21} & \tilde{\varepsilon}_2 \end{pmatrix} + \begin{pmatrix} \tilde{V}_{1B} \\ \tilde{V}_{2B} \end{pmatrix} \frac{1}{E - \tilde{\varepsilon}_B} (\tilde{V}_{B1}\ \tilde{V}_{B2}) \tag{15}$$

Here, the parameter E corresponds to the adiabatic energy and is calculated as an eigenvalue of H^{eff} (taking the lower eigenvalue for holes and the higher one for electrons). Since the H^{eff} matrix is also dependent on E, the final value of E is obtained by a self-consistent iterative procedure. After further unitary transformation, the effective electronic coupling is written as

$$V_{12}^{\text{eff}} = \tilde{V}_{12} + \sum_{b \in B} \frac{\tilde{U}_b^+ \tilde{V}_{1B} \tilde{V}_{B2} \tilde{U}_b}{\tilde{U}_b^+ (E - \tilde{\varepsilon}_B) \tilde{U}_b} = \tilde{V}_{12} + \sum_{b \in B} \frac{\tilde{V}_{1b} \tilde{V}_{b2}}{E - \tilde{\varepsilon}_b} \tag{16}$$

Here, $\tilde{\varepsilon}_b$ and $\tilde{U}_b$ are the eigenvalues and eigenvectors of the bridge block matrix $\tilde{\varepsilon}_B$, respectively. From eq 16, the contribution of each molecular level of the bridge can be clarified by the partition-based method, which is useful to reveal the origin of the superexchange coupling.

To illustrate the importance of the polarization effect, Figure 3 shows the superexchange couplings as a function of the longitude displacement of the middle bridge in the DAD and ADA triads extracted from the experimental PTZ−TCNQ (PTZ = phenothiazine, TCNQ = 7,7,8,8-tetracyanoquinodimethane) crystal.[54] When the displacement increases, the couplings calculated by the partition-based method are continuously decreased for both holes and electrons. At the experimental symmetric geometries, the coupling values estimated by the energy splitting method are in good agreement with those by the partition-based method. However, as the middle bridge is displaced, the energy-splitting estimates will deviate from the results obtained by the partition-based method and the overall trends are even wrong due to lack of considering the site energy difference that arises from the symmetry breaking of the triad geometries. Therefore, the difference of the calculated couplings between the two methods can be very large even at a small displacement; the partition-based method is imperative in the studies of nonlocal electron−phonon couplings and disordered systems.[55]

3. ORIGIN OF CHARGE CARRIER POLARITIES: THE ROLE OF SUPEREXCHANGE CHANNELS

Organic semiconductors with different charge carrier polarities are requisite for organic electronics and complementary electrical circuits. Currently, both hole- and electron-dominant as well as ambipolar transport have been reported in the D−A mixed-stack crystals and copolymers. Here, we take several molecular cocrystal systems as examples to elucidate the charge carrier polarities in terms of the superexchange couplings (see Figure 4a).[14] For the PAZ−PMA (PAZ = phenazine, PMA = pyromellitic dianhydride) mixed-stack crystal,[56] the superexchange coupling for holes (33 meV) is stronger than that for electrons (21 meV); thus, hole transport is expected to be dominant. In contrast, for the CHR (chrysene)−TCNQ cocrystal,[57] the superexchange coupling for holes is vanishingly small (2 meV), while that for electrons can be as large as 47 meV, indicating an excellent electron transport. Interestingly, in the case of the PTZ−TCNQ cocrystal,[54] balanced and large couplings (71 meV) are found for holes and electrons, implying remarkable ambipolar charge transport.

To gain an in-depth understanding of the origin of different charge polarities, we analyzed the contribution of each bridge molecular orbital. As shown in Figure 4b and c, the superexchange interaction is controlled by a very limited number of bridge orbitals. In the case of PTZ−TCNQ, the superexchange couplings for holes and electrons are both dictated exclusively by the interaction between the HOMO of the PTZ donor and the LUMO of the TCNQ acceptor; namely, the same nature of superexchange interaction is found for hole and electron transport, thus leading to almost equivalent couplings. For PAZ−PMA, besides the HOMO, another occupied orbital (HOMO−3) of the bridge PAZ molecule can also play an important role for electron transport. In addition, the HOMO and HOMO−3 of the PAZ donor display opposite symmetries and are both lying below the LUMO of the PMA acceptor; therefore, the contributions of these two orbitals of PAZ to the superexchange coupling for electrons cancel out each other. For hole transport, the essential bridge orbitals of the LUMO and HOMO−12 of the PMA acceptor simultaneously exhibit opposite symmetries and relative energies with respect to the HOMO of the PAZ donor, so these two bridge orbitals play a constructive role in mediating the superexchange coupling for holes. Consequently, the electronic coupling for holes is relatively stronger than that for electrons. In the case of CHR−TCNQ, the displacement between CHR and TCNQ along the short molecular axis is very small. As a result, the wave function overlap between the HOMO of CHR and the LUMO of TCNQ vanishes due to the different symmetries of these two orbitals along the short axis. In contrast, the HOMO−1 of CHR can strongly interact with the LUMO of TCNQ due to the same symmetry along the short axis. Thus, the HOMO−1 of CHR can mediate a significant superexchange coupling for electron transfer between the TCNQ molecules (47 meV), whereas the superexchange coupling for hole transfer between the CHR molecules (2 meV) is extremely small due to lack of effective bridge orbital channels, leading to a unipolar electron transport in CHR−TCNQ. Interestingly, due to a similar reason, electron-dominant charge transport has been demonstrated in other TCNQ-based cocrytals using acenes, phenes, and thienoacenes as donors.[17,58]

Similar to the D−A mixed-stack cocrystals, the intrachain charge transport of D−A copolymers can also arise from the superexchange mechanism.[47] With the progress in material processing techniques, polymer nanowires and highly crystalline thin films have been prepared and remarkably high mobilitis have been demonstrated.[38] Therefore, the D−A copolymer backbone can be approximately regarded as a one-dimensional periodic structure. In spite of the covalent connection between the donor and acceptor fragments, the molecular orbitals of the entire copolymer chain can be approximated as a linear combination of the orbitals of donor and acceptor fragments.

It should be noted that the covalent bonding can result in strong polarization between the donor and acceptor segments. Usually, the polarized HOMO and LUMO energies of the acceptor segments are all lower than those of the donor

DOI: 10.1021/acs.chemmater.9b01545
Chem. Mater. 2019, 31, 6424−6434

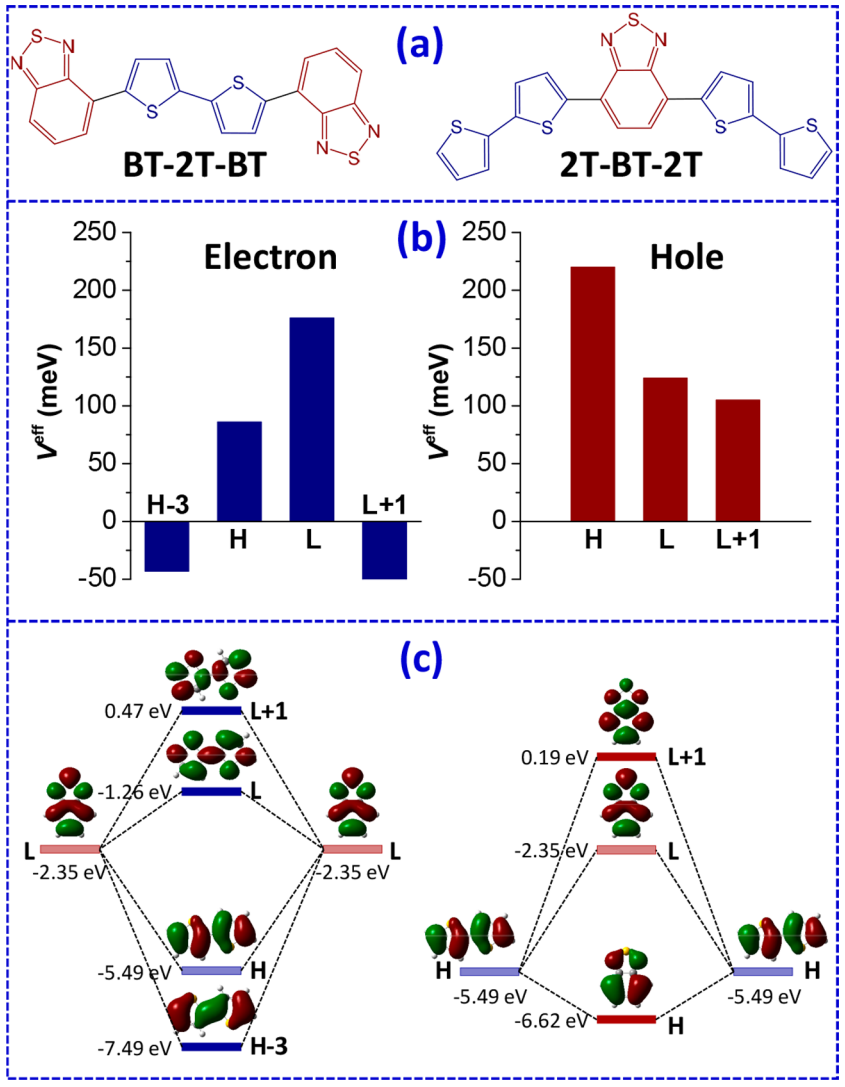

Figure 5. (a) Illustration of the DAD and ADA triad models; (b) contributions of essential bridge orbitals to the superexchange couplings; (c) important molecular orbitals of the donor and acceptor components involved in the superexchange interaction for the 2T−BT copolymer.

segments, presenting a staggered type of energy alignment between donor and acceptor. The hole and electron carriers are expected to be mainly localized on the donor and acceptor segments, respectively. Therefore, the DAD and ADA triad models are used to calculate the superexchange couplings for holes and electrons, respectively. Since the donor HOMO lies within the HOMO−LUMO gap of the acceptor and the acceptor LUMO is also within the HOMO−LUMO gap of the donor, both the HOMO and LUMO levels of the bridges can play an important role in mediating superexchange charge transport. We also note that, in some cases, both the HOMO and LUMO levels of the acceptor segments are lying between the HOMO and LUMO levels of the donor segments; then, both the electron and hole carriers tend to reside on the acceptor segments, and the superexchange couplings for holes and electrons should be calculated by using the same ADA triad model.

For the 2T−BT copolymer, the HOMO of the 2T donor lies between the HOMO and LUMO of the BT acceptor and the LUMO of BT is also within the HOMO−LUMO gap of 2T, so the superexchange couplings can be calculated using the 2T−BT−2T triad for holes and using the BT−2T−BT for electrons (Figure 5a). As expected, both the HOMO and LUMO levels of the bridge play the most important role in superexchange transport for holes and electrons (Figure 5b). For hole transport, the LUMO+1 of BT is also an essential bridge channel. Especially, the LUMO and LUMO+1 of BT are both antisymmetric along the covalent connection direction while the HOMO of BT is symmetric, so these three key bridge channels play a constructive role in the hole transport and the superexchange coupling for holes (ca. 380 meV) is maximized. In the case of electron transport, there are two additional important channels for 2T as a bridge, i.e., the LUMO+1 (symmetric) and HOMO−3 (antisymmetric), which are of inverse symmetries compared with the LUMO (antisymmetric) and HOMO (symmetric), respectively. Thus, the LUMO +1 and HOMO−3 of the 2T bridge are destructive to the superexchange interaction and the coupling for electrons (ca. 170 meV) is much reduced with respect to that for holes. Therefore, the 2T−BT copolymer will present a hole-dominant transport polarity. To conclude, the relative phases of bridge orbitals and the relative energy alignments determine constructive or destructive interference to the total super-

DOI: 10.1021/acs.chemmater.9b01545
Chem. Mater. 2019, 31, 6424−6434

Scheme 2. Illustration of the Energy Alignments between the DTDPP and *n*T Segments and the Corresponding Triad Models for the Superexchange Couplings for Holes and Electrons in the DTDPP−*n*T Copolymers

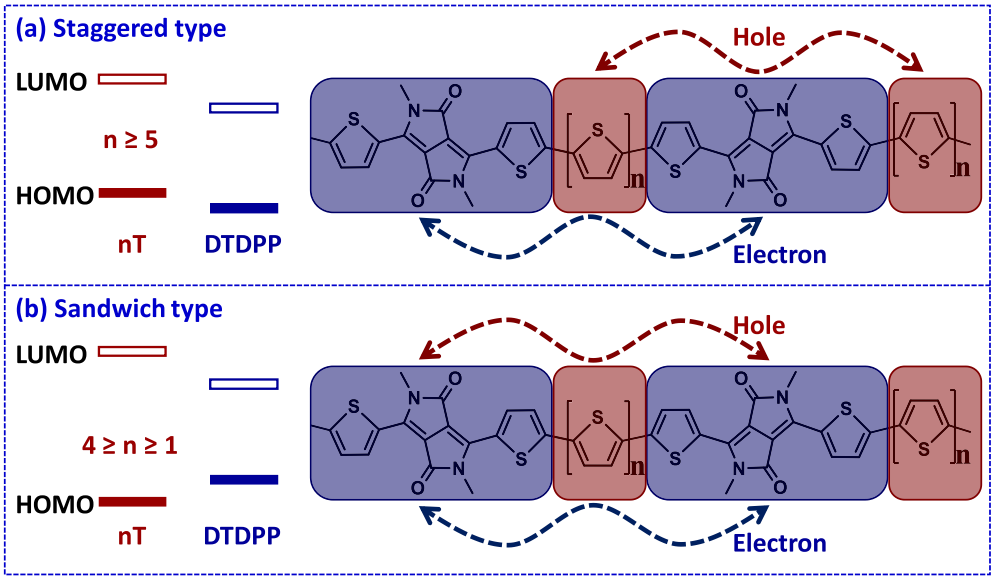

exchange coupling; different charge transfer polarities can be obtained by modifying the role of bridge orbitals.[17,22]

For the DTDPP−*n*T copolymers, the acceptor segment of DTDPP has a narrow HOMO−LUMO gap due to the relatively high HOMO level and low LUMO level. As the number of thiophene units (n) in the donor segment is decreased, the HOMO−LUMO gap of the *n*T donor will be enlarged and it easily turns to cover both the HOMO and LUMO levels of the DTDPP segment from $n = 5$ to $n = 4$ or less (Scheme 2). Then, the relative energy alignment between the donor and acceptor segments is changed from a staggered type for DTDPP−5T to a sandwich type for DTDPP−*n*T, $1 \leq n \leq 4$. In the latter case, no matter for electrons or for holes, the superexchange coupling is based on the same ADA triad model (Scheme 2b); this would be beneficial for achieving the ambipolar charge transport polarity.[46]

4. MODULATION OF SUPEREXCHANGE COUPLING BY D−A INTERACTION

As described above, the long-range superexchange mechanism can make ultrasmall effective masses and high charge transport performance for D−A cocrystals and copolymers. The magnitude of the superexchange coupling is determined by the D−A energy alignment and electronic interaction. However, owing to different interaction modes between the donor and the acceptor, D−A cocrystals and copolymers present a distinct modulation dependence on molecular structures. For D−A cocrystals, the D−A electronic couplings originate from the orbital overlaps, which are closely related to the nodes and phases of the molecular orbitals.

As seen from Figure 6a, the D−A electronic couplings of the essential bridge orbitals are very strong, with the largest absolute values >300 meV. This is attributed to a synergistic effect of the overlaps between the donor and acceptor wave functions at different positions, especially for the (PTZ HOMO)−(TCNQ LUMO), (CHR HOMO−1)−(TCNQ LUMO), and (PAZ HOMO)−(PMA LUMO) pairs. As mentioned previously, the CHR HOMO reveals an antibonding mode while the TCNQ LUMO presents a bonding mode

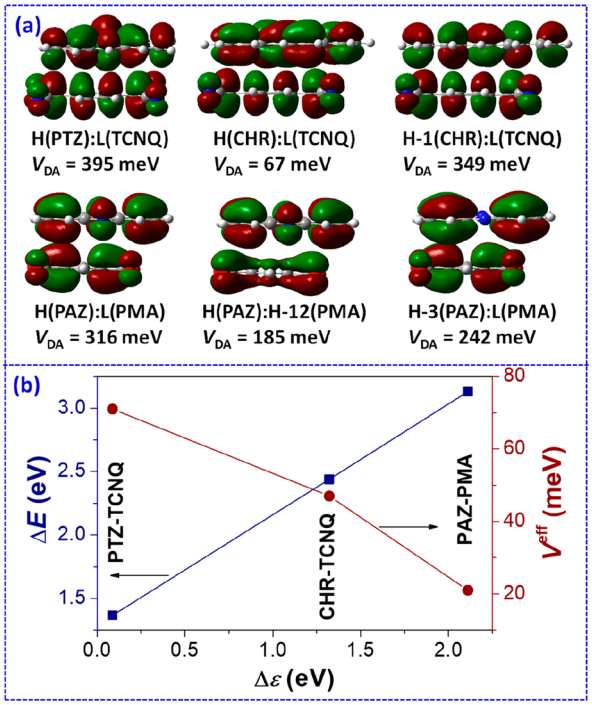

Figure 6. (a) Representation of molecular orbitals of the donor and acceptor moieties in D−A dyads along the stacking direction (H, HOMO; L, LUMO); (b) dependence of the energy difference (ΔE) between the adiabatic and bridge levels in the trimer and the superexchange coupling for electrons on the orbital energy offset ($\Delta\varepsilon$) of isolated donors and acceptors.

in the lateral direction; thus, the orbital overlaps almost compensate each other in this direction for the CHR−TCNQ dyad. Consequently, the electronic coupling between the CHR HOMO and the TCNQ LUMO (67 meV) is merely one-fifth of the largest one. From Figure 6a, we can also see that a small intermolecular shift may significantly change the D−A electronic interaction and the superexchange couplings.

DOI: 10.1021/acs.chemmater.9b01545
Chem. Mater. 2019, 31, 6424−6434

On the condition of similar D−A couplings, we can investigate the impact of D−A energy alignments on the superexchange couplings. It was found that the orbital energy offset of an isolated donor and acceptor presents a good linear relationship with the polarized energy difference between the adiabatic and bridge levels in the trimer. The superexchange coupling is then inversely proportional to the orbital energy offset of an isolated donor and acceptor (see Figure 6b). It should be noticed that various charge transport properties have been achieved in experiments through modulating the energy alignments between the donor and acceptor.[1,21,58]

For better understanding of the superexchange couplings of D−A copolymers, the explicit term, i.e., the second term in eq 13, can be rewritten under the tight binding Hückel approximation as follows:

$$V_{h/e}^{eff} \propto C_{HOMO/LUMO}^{1(B)} C_{HOMO/LUMO}^{2(B)} \cos(\varphi_{1B}) \cos(\varphi_{B2}) \sum_{\nu \in B} \frac{C_\nu^{B(1)} C_\nu^{B(2)}}{E - \varepsilon_\nu^B} \quad (17)$$

Here, $C_{HOMO/LUMO}^{1(B)}$ or $C_{HOMO/LUMO}^{2(B)}$ denotes the HOMO/LUMO coefficients of monomer 1 or monomer 2 at the atoms connecting with the middle bridge; $C_\nu^{B(1)}$ or $C_\nu^{B(2)}$ represents the coefficient of bridge orbital ν at the atoms connecting with monomer 1 or monomer 2; φ_{1B} or φ_{B2} is the torsional angle of the bridge with respect to monomer 1 or monomer 2; E and ε_ν^B correspond to the energy of the adiabatic orbital of the (monomer 1)−bridge−(monomer 2) triad and the energy of bridge orbital ν, respectively. In the case of symmetric triad systems, $C_{HOMO/LUMO}^{1(B)} C_{HOMO/LUMO}^{2(B)} = \rho_{HOMO/LUMO}^{1(B)} = \rho_{HOMO/LUMO}^{2(B)}$ and $\varphi_{1B} = \varphi_{B2}$, then the superexchange coupling depends on the charge densities at the linkage sites and torsional angles between the donor and acceptor segments (see Figure 7a).

A series of combinations of electron-deficient moieties and electron-rich moieties were investigated to reveal the molecular factors that influence superexchange couplings in D−A copolymers. The electron-deficient moieties include IID (isoindigo), BT (benzothiadiazole), PT (pyridal[2,1,3]-thiadiazole), TDQ ([1,2,5]thiadiazolo[3,4-g]quinoxaline), 4FPh (tetra-fluorophenylene), and $(CF_2)_4$, and the electron-rich moieties include Py (pyrene), Flu (fluorene), 2T (dithiophene), 4T (tetra-thiophene), TTTT (four-fused thiophene), TVT ((*E*)-2-(2-(thiophen-2-yl)vinyl) thiophene), IDT (indacenodithiophene), and CDT (cyclopentadithiophene). It should be mentioned that the CDT−PT copolymer presents the highest mobility among polymeric semiconductors, reaching ~50 $cm^2\ V^{-1}\ s^{-1}$ measured by using FET devices.[38] Owing to the big steric effect, large torsional angles present in the IID-, Flu-, and Py-based copolymers and thereby the superexchange couplings are relatively small. As seen in Figure 7b, the hole superexchange coupling is linearly increased with the projected electron density of the HOMO at the linkage site, consistent with the prediction from eq 14. It should be noticed that, for the Py-based copolymer, there is almost no electron density distribution on the linking carbon atoms for the HOMO of Py due to the symmetry forbidden (namely, the linkage atom is at the orbital node); thus, the superexchange coupling is extremely small and large effective mass is found for these copolymers. In sharp contrast, the electron densities at the linkage atoms are the highest for the CDT moiety; thus, the CDT-based copolymers display the largest superexchange

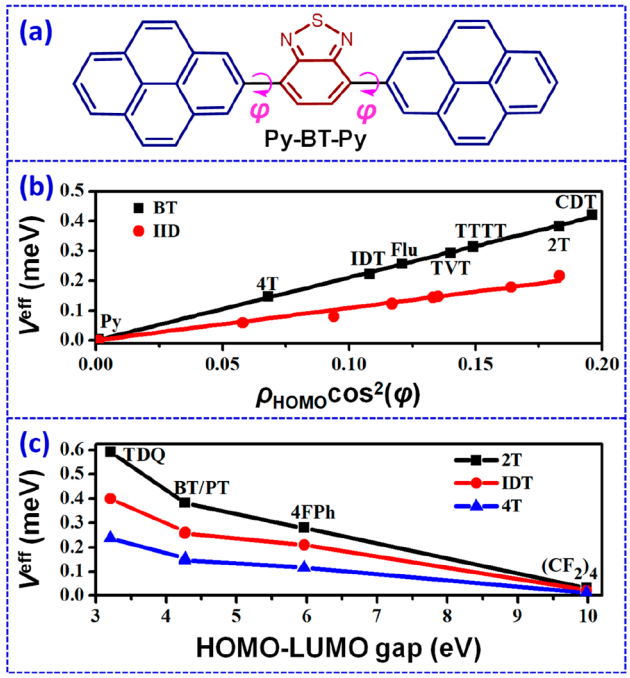

Figure 7. (a) Illustration of the DAD triad for the hole superexchange coupling and the dihedral angles between the donor and acceptor units using the Py−BT copolymer as an example; (b) dependence of the hole superexchange couplings on the HOMO electron densities at the linkage atom of the donor units and the dihedral angles; (c) dependence of the hole superexchange couplings on the HOMO−LUMO gaps of the bridges of acceptors.

couplings. Since the transport level is usually between the HOMO and LUMO levels of the bridge, the HOMO−LUMO gap of the bridge can greatly influence the superexchange coupling. As seen in Figure 7c, the superexchange coupling is continuously decreased with the increasing HOMO−LUMO gap. Because of the smallest HOMO−LUMO gap, the TDQ-based copolymers exhibit the largest superexchange couplings. On the contrary, the superexchange couplings are the smallest for the $(CF_2)_4$-based copolymers due to the biggest HOMO−LUMO gap. As the superexchange couplings are strongly correlated to the measured charge mobilities and larger superexchange couplings can result in higher charge mobilities at a given distance,[47] it is crucial to decrease the bandgaps and increase the frontier orbital electron densities on the linking atoms of the donor and acceptor units for the design of high-performance copolymers.

5. CONCLUSIONS AND OUTLOOK

We have extended the superexchange mechanism, which was initially used to explain the long-range photoinduced electron transfer in DNA,[59] to the charge transport properties in organic mixed systems, such as D−A cocrystals and copolymers. On the basis of a DAD or ADA triad, the superexchange couplings can be derived. From the superexchange perspective, the charge carrier polarities of D−A cocrystals and copolymers are dependent on the relative phases of the middle bridge orbitals and their relative energies compared to the transporting levels. The magnitudes of the superexchange couplings are determined by the electronic couplings and energy alignments between the donor and acceptor segments. Specifically, the superexchange couplings of D−A cocrystals can be changed by modulation of the

DOI: 10.1021/acs.chemmater.9b01545
Chem. Mater. 2019, 31, 6424−6434

intermolecular distances and displacements between the donor and acceptor molecules. In order to enhance the superexchange couplings of D−A copolymers, the electron densities at the linkage atoms of the frontier orbitals of the donor and acceptor moieties need to be maximized and the torsional angles between the donor and acceptor moieties should be minimized. These findings are very useful to obtain high-mobility organic semiconductors with desired charge carrier polarities.

At present, the superexchange mechanism has also been demonstrated in the charge transport of multicomponent disordered organic semiconductors. For instance, the charge transport can be significantly enhanced by superexchange in the emissive host−guest layers of OLEDs and in the D−A active layers of organic solar cells.[60−63] Especially when the dopant molecules act as relatively deep trap states, superexchange can increase the charge-transfer rate between them and result in a percolating network for charge transport at low concentrations. Therefore, it can be anticipated that superexchange charge transport is common in organic optoelectronic materials and can play an important role for the device performance.

AUTHOR INFORMATION

Corresponding Authors

*E-mail: ypyi@iccas.ac.cn.
*E-mail: zgshuai@tsinghua.edu.cn.

ORCID

Hua Geng: 0000-0001-6485-1339
Yuanping Yi: 0000-0002-0052-9364
Daoben Zhu: 0000-0002-6354-940X
Zhigang Shuai: 0000-0003-3867-2331

Notes

The authors declare no competing financial interest.

ACKNOWLEDGMENTS

This work is supported by National Key R&D Program of China (2017YFA0204700, 2017YFA0204502) and the National Natural Science Foundation of China (21673247, 21473043), Beijing Municipal Natural Science Foundation (2182012, 2192013) and Capacity Building for Sci-Tech Innovation-Fundamental Scientific Research Funds (19530050138), and the Strategic Priority Research Program of the Chinese Academy of Sciences (XDB12020200).

REFERENCES

(1) Zhang, J.; Xu, W.; Sheng, P.; Zhao, G.; Zhu, D. Organic Donor-Acceptor Complexes as Novel Organic Semiconductors. *Acc. Chem. Res.* **2017**, *50*, 1654−1662.

(2) Lei, Y.-L.; Jin, Y.; Zhou, D.-Y.; Gu, W.; Shi, X.-B.; Liao, L.-S.; Lee, S.-T. White-Light Emitting Microtubes of Mixed Organic Charge-Transfer Complexes. *Adv. Mater.* **2012**, *24*, 5345−5351.

(3) Park, S. K.; Kim, J. H.; Ohto, T.; Yamada, R.; Jones, A. O. F.; Whang, D. R.; Cho, I.; Oh, S.; Hong, S. H.; Kwon, J. E.; Kim, J. H.; Olivier, Y.; Fischer, R.; Resel, R.; Gierschner, J.; Tada, H.; Park, S. Y. Highly Luminescent 2D-Type Slab Crystals Based on a Molecular Charge-Transfer Complex as Promising Organic Light-Emitting Transistor Materials. *Adv. Mater.* **2017**, *29*, 1701346.

(4) Sun, L.; Zhu, W.; Yang, F.; Li, B.; Ren, X.; Zhang, X.; Hu, W. Molecular cocrystals: design, charge-transfer and optoelectronic functionality. *Phys. Chem. Chem. Phys.* **2018**, *20*, 6009−6023.

(5) Zhang, J.; Jin, J.; Xu, H.; Zhang, Q.; Huang, W. Recent progress on organic donor-acceptor complexes as active elements in organic field-effect transistors. *J. Mater. Chem. C* **2018**, *6*, 3485−3498.

(6) d'Agostino, S.; Spinelli, F.; Taddei, P.; Ventura, B.; Grepioni, F. Ultralong Organic Phosphorescence in the Solid State: The Case of Triphenylene Cocrystals with Halo-and Dihalo-penta/tetrafluorobenzene. *Cryst. Growth Des.* **2019**, *19*, 336−346.

(7) Zhu, L.; Yi, Y.; Li, Y.; Kim, E.-G.; Coropceanu, V.; Brédas, J.-L. Prediction of Remarkable Ambipolar Charge-Transport Characteristics in Organic Mixed-Stack Charge-Transfer Crystals. *J. Am. Chem. Soc.* **2012**, *134*, 2340−2347.

(8) Zhang, J.; Geng, H.; Virk, T. S.; Zhao, Y.; Tan, J.; Di, C.-a.; Xu, W.; Singh, K.; Hu, W.; Shuai, Z.; Liu, Y.; Zhu, D. Sulfur-Bridged Annulene-TCNQ Co-Crystal: A Self-Assembled "Molecular Level Heterojunction" with Air Stable Ambipolar Charge Transport Behavior. *Adv. Mater.* **2012**, *24*, 2603−2607.

(9) Wakahara, T.; D'Angelo, P.; Miyazawa, K. I.; Nemoto, Y.; Ito, O.; Tanigaki, N.; Bradley, D. D. C.; Anthopoulos, T. D. Fullerene/Cobalt Porphyrin Hybrid Nanosheets with Ambipolar Charge Transporting Characteristics. *J. Am. Chem. Soc.* **2012**, *134*, 7204−7206.

(10) Zhang, J.; Tan, J.; Ma, Z.; Xu, W.; Zhao, G.; Geng, H.; Di, C. A.; Hu, W.; Shuai, Z.; Singh, K.; Zhu, D. Fullerene/sulfur-bridged annulene cocrystals: two-dimensional segregated heterojunctions with ambipolar transport properties and photoresponsivity. *J. Am. Chem. Soc.* **2013**, *135*, 558−561.

(11) Wu, H.-D.; Wang, F.-X.; Xiao, Y.; Pan, G.-B. Preparation and ambipolar transistor characteristics of co-crystal microrods of dibenzotetrathiafulvalene and tetracyanoquinodimethane. *J. Mater. Chem. C* **2013**, *1*, 2286−2289.

(12) Park, S. K.; Varghese, S.; Kim, J. H.; Yoon, S.-J.; Kwon, O. K.; An, B.-K.; Gierschner, J.; Park, S. Y. Tailor-Made Highly Luminescent and Ambipolar Transporting Organic Mixed Stacked Charge-Transfer Crystals: An Isometric Donor-Acceptor Approach. *J. Am. Chem. Soc.* **2013**, *135*, 4757−4764.

(13) Zhu, L.; Yi, Y.; Fonari, A.; Corbin, N. S.; Coropceanu, V.; Brédas, J.-L. Electronic Properties of Mixed-Stack Organic Charge-Transfer Crystals. *J. Phys. Chem. C* **2014**, *118*, 14150−14156.

(14) Geng, H.; Zheng, X.; Shuai, Z.; Zhu, L.; Yi, Y. Understanding the Charge Transport and Polarities in Organic Donor-Acceptor Mixed-Stack Crystals: Molecular Insights from the Super-Exchange Couplings. *Adv. Mater.* **2015**, *27*, 1443−1449.

(15) Jin, J.; Long, G.; Gao, Y.; Zhang, J.; Ou, C.; Zhu, C.; Xu, H.; Zhao, J.; Zhang, M.; Huang, W. Supramolecular Design of Donor-Acceptor Complexes via Heteroatom Replacement toward Structure and Electrical Transporting Property Tailoring. *ACS Appl. Mater. Interfaces* **2019**, *11*, 1109−1116.

(16) Mandal, A.; Swain, P.; Nath, B.; Sau, S.; Mal, P. Unipolar to ambipolar semiconductivity switching in charge transfer cocrystals of 2,7-di-tert-butylpyrene. *CrystEngComm* **2019**, *21*, 981−989.

(17) Iijima, K.; Sanada, R.; Yoo, D.; Sato, R.; Kawamoto, T.; Mori, T. Carrier Charge Polarity in Mixed-Stack Charge-Transfer Crystals Containing Dithienobenzodithiophene. *ACS Appl. Mater. Interfaces* **2018**, *10*, 10262−10269.

(18) Zhang, J.; Liu, G.; Zhou, Y.; Long, G.; Gu, P.; Zhang, Q. Solvent Accommodation: Functionalities Can Be Tailored Through Co-Crystallization Based on 1:1 Coronene-F4TCNQ Charge-Transfer Complex. *ACS Appl. Mater. Interfaces* **2017**, *9*, 1183−1188.

(19) Sato, R.; Dogishi, M.; Higashino, T.; Kadoya, T.; Kawamoto, T.; Mori, T. Charge-Transfer Complexes of Benzothienobenzothiophene with Tetracyanoquinodimethane and the n-Channel Organic Field-Effect Transistors. *J. Phys. Chem. C* **2017**, *121*, 6561−6568.

(20) Hu, P.; Li, H.; Li, Y.; Jiang, H.; Kloc, C. Single-crystal growth, structures, charge transfer and transport properties of anthracene-F4TCNQ and tetracene-F4TCNQ charge-transfer compounds. *CrystEngComm* **2017**, *19*, 618−624.

(21) Qin, Y.; Cheng, C.; Geng, H.; Wang, C.; Hu, W.; Xu, W.; Shuai, Z.; Zhu, D. Efficient ambipolar transport properties in alternate

DOI: 10.1021/acs.chemmater.9b01545
Chem. Mater. 2019, 31, 6424−6434

stacking donor-acceptor complexes: from experiment to theory. *Phys. Chem. Chem. Phys.* **2016**, *18*, 14094−14103.
(22) Goetz, K. P.; Tsutsumi, J. Y.; Pookpanratana, S.; Chen, J.; Corbin, N. S.; Behera, R. K.; Coropceanu, V.; Richter, C. A.; Hacker, C. A.; Hasegawa, T.; Jurchescu, O. D. Polymorphism in the 1:1 Charge-Transfer Complex DBTTF-TCNQ and Its Effects on Optical and Electronic Properties. *Adv. Electron. Mater.* **2016**, *2*, 1600203.
(23) Zhang, J.; Gu, P.; Long, G.; Ganguly, R.; Li, Y.; Aratani, N.; Yamada, H.; Zhang, Q. Switching charge-transfer characteristics from p-type to n-type through molecular "doping" (co-crystallization). *Chem. Sci.* **2016**, *7*, 3851−3856.
(24) Higashino, T.; Dogishi, M.; Kadoya, T.; Sato, R.; Kawamoto, T.; Mori, T. Air-stable n-channel organic field-effect transistors based on charge-transfer complexes including dimethoxybenzothienobenzothiophene and tetracyanoquinodimethane derivatives. *J. Mater. Chem. C* **2016**, *4*, 5981−5987.
(25) Zhu, W.; Yi, Y.; Zhen, Y.; Hu, W. Precisely Tailoring the Stoichiometric Stacking of Perylene-TCNQ Co-Crystals towards Different Nano and Microstructures with Varied Optoelectronic Performances. *Small* **2015**, *11*, 2150−2156.
(26) Wu, H.-D.; Wang, F.-X.; Zhang, M.; Pan, G.-B. Investigation of transport properties of coronene·TCNQ cocrystal microrods with coronene microrods and TCNQ microsheets. *Nanoscale* **2015**, *7*, 12839−12842.
(27) Tsutsumi, J.; Matsuoka, S.; Inoue, S.; Minemawari, H.; Yamada, T.; Hasegawa, T. N-Type Field-Effect Transistor Based on Layered Crystalline Donor-Acceptor Semiconductors with Dialkylated Benzothienobenzothiophenes as Electron Donors. *J. Mater. Chem. C* **2015**, *3*, 1976−1981.
(28) Su, Y.; Li, Y.; Liu, J.; Xing, R.; Han, Y. Donor-acceptor cocrystal based on hexakis(alkoxy)triphenylene and perylenediimide derivatives with an ambipolar transporting property. *Nanoscale* **2015**, *7*, 1944−1955.
(29) Shibata, Y.; Tsutsumi, J.; Apos; Ya; Matsuoka, S.; Matsubara, K.; Yoshida, Y.; Chikamatsu, M.; Hasegawa, T. Uniaxially oriented polycrystalline thin films and air-stable n-type transistors based on donor-acceptor semiconductor (diC8BTBT)(FnTCNQ) [n = 0, 2, 4]. *Appl. Phys. Lett.* **2015**, *106*, 143303.
(30) Zhang, J.; Zhao, G.; Qin, Y.; Tan, J.; Geng, H.; Xu, W.; Hu, W.; Shuai, Z.; Zhu, D. Enhancement of the p-channel performance of sulfur-bridged annulene through a donor-acceptor co-crystal approach. *J. Mater. Chem. C* **2014**, *2*, 8886−8891.
(31) Mahns, B.; Kataeva, O.; Islamov, D.; Hampel, S.; Steckel, F.; Hess, C.; Knupfer, M.; Büchner, B.; Himcinschi, C.; Hahn, T.; Renger, R.; Kortus, J. Crystal Growth, Structure, and Transport Properties of the Charge-Transfer Salt Picene/2,3,5,6-Tetrafluoro-7,7,8,8-tetracyanoquinodimethane. *Cryst. Growth Des.* **2014**, *14*, 1338−1346.
(32) Vermeulen, D.; Zhu, L. Y.; Goetz, K. P.; Hu, P.; Jiang, H.; Day, C. S.; Jurchescu, O. D.; Coropceanu, V.; Kloc, C.; McNeil, L. E. Charge Transport Properties of Perylene-TCNQ Crystals: The Effect of Stoichiometry. *J. Phys. Chem. C* **2014**, *118*, 24688−24696.
(33) Qin, Y.; Zhang, J.; Zheng, X.; Geng, H.; Zhao, G.; Xu, W.; Hu, W.; Shuai, Z.; Zhu, D. Charge-transfer complex crystal based on extended-pi-conjugated acceptor and sulfur-bridged annulene: charge-transfer interaction and remarkable high ambipolar transport characteristics. *Adv. Mater.* **2014**, *26*, 4093−4099.
(34) Venkateshvaran, D.; Nikolka, M.; Sadhanala, A.; Lemaur, V.; Zelazny, M.; Kepa, M.; Hurhangee, M.; Kronemeijer, A. J.; Pecunia, V.; Nasrallah, I.; Romanov, I.; Broch, K.; McCulloch, I.; Emin, D.; Olivier, Y.; Cornil, J.; Beljonne, D.; Sirringhaus, H. Approaching disorder-free transport in high-mobility conjugated polymers. *Nature* **2014**, *515*, 384−388.
(35) Kim, G.; Kang, S. J.; Dutta, G. K.; Han, Y. K.; Shin, T. J.; Noh, Y. Y.; Yang, C. A thienoisoindigo-naphthalene polymer with ultrahigh mobility of 14.4 cm(2)/V.s that substantially exceeds benchmark values for amorphous silicon semiconductors. *J. Am. Chem. Soc.* **2014**, *136*, 9477−9483.
(36) Kim, G.; Han, A. R.; Lee, H. R.; Lee, J.; Oh, J. H.; Yang, C. Acceptor-acceptor type isoindigo-based copolymers for high-performance n-channel field-effect transistors. *Chem. Commun.* **2014**, *50*, 2180−2183.
(37) Yang, J.; Zhao, Z.; Geng, H.; Cheng, C.; Chen, J.; Sun, Y.; Shi, L.; Yi, Y.; Shuai, Z.; Guo, Y.; Wang, S.; Liu, Y. Isoindigo-Based Polymers with Small Effective Masses for High-Mobility Ambipolar Field-Effect Transistors. *Adv. Mater.* **2017**, *29*, 1702115.
(38) Luo, C.; Kyaw, A. K.; Perez, L. A.; Patel, S.; Wang, M.; Grimm, B.; Bazan, G. C.; Kramer, E. J.; Heeger, A. J. General strategy for self-assembly of highly oriented nanocrystalline semiconducting polymers with high mobility. *Nano Lett.* **2014**, *14*, 2764−2771.
(39) Yuen, J. D.; Fan, J.; Seifter, J.; Lim, B.; Hufschmid, R.; Heeger, A. J.; Wudl, F. High Performance Weak Donor-Acceptor Polymers in Thin Film Transistors: Effect of the Acceptor on Electronic Properties, Ambipolar Conductivity, Mobility, and Thermal Stability. *J. Am. Chem. Soc.* **2011**, *133*, 20799−20807.
(40) Lee, J.; Chung, J. W.; Kim, D. H.; Lee, B. L.; Park, I. I.; Lee, S.; Hausermann, R.; Batlogg, B.; Lee, S. S.; Choi, I.; Kim, I. W.; Kang, M. S. Thin Films of Highly Planar Semiconductor Polymers Exhibiting Band-like Transport at Room Temperature. *J. Am. Chem. Soc.* **2015**, *137*, 7990−7993.
(41) Sun, B.; Hong, W.; Yan, Z. Q.; Aziz, H.; Li, Y. N. Record High Electron Mobility of 6.3 $cm^2V^{-1}s^{-1}$ Achieved for Polymer Semiconductors Using a New Building Block. *Adv. Mater.* **2014**, *26*, 2636−2642.
(42) Yun, H. J.; Kang, S. J.; Xu, Y.; Kim, S. O.; Kim, Y. H.; Noh, Y. Y.; Kwon, S. K. Dramatic Inversion of Charge Polarity in Diketopyrrolopyrrole-Based Organic Field-Effect Transistors via a Simple Nitrile Group Substitution. *Adv. Mater.* **2014**, *26*, 7300−7307.
(43) Yi, Z. R.; Ma, L. C.; Chen, B.; Chen, D. G.; Chen, X. G.; Qin, J. G.; Zhan, X. W.; Liu, Y. Q.; Ong, W. J.; Li, J. Effect of the Longer beta-Unsubstituted Oliogothiophene Unit (6T and 7T) on the Organic Thin-Film Transistor Performances of Diketopyrrolopyrrole-Oliogothiophene Copolymers. *Chem. Mater.* **2013**, *25*, 4290−4296.
(44) Lee, J.; Han, A. R.; Yu, H.; Shin, T. J.; Yang, C.; Oh, J. H. Boosting the Ambipolar Performance of Solution-Processable Polymer Semiconductors via Hybrid Side-Chain Engineering. *J. Am. Chem. Soc.* **2013**, *135*, 9540−9547.
(45) Fornari, R. P.; Troisi, A. Narrower Bands with Better Charge Transport: The Counterintuitive Behavior of Semiconducting Copolymers. *Adv. Mater.* **2014**, *26*, 7627−7631.
(46) He, F.; Cheng, C.; Geng, H.; Yi, Y.; Shuai, Z. Effect of donor length on electronic structures and charge transport polarity for DTDPP-based D-A copolymers: a computational study based on a super-exchange model. *J. Mater. Chem. A* **2018**, *6*, 11985−11993.
(47) Cheng, C.; Geng, H.; Yi, Y.; Shuai, Z. Super-exchange-induced high performance charge transport in donor-acceptor copolymers. *J. Mater. Chem. C* **2017**, *5*, 3247−3253.
(48) Hotta, S.; Kobayashi, H. Crystal and Molecular-Structure of a Charge-Transfer Complex between α,α'-Dimethylquaterthiophene and 2,3,5,6-Tetrafluoro-7,7,8,8-Tetracyanoquinodimethane. *Synth. Met.* **1994**, *66*, 117−122.
(49) Coropceanu, V.; Cornil, J.; da Silva Filho, D. A.; Olivier, Y.; Silbey, R.; Brédas, J.-L. Charge Transport in Organic Semiconductors. *Chem. Rev.* **2007**, *107*, 926−952.
(50) Brédas, J. L.; Calbert, J. P.; da Silva Filho, D. A.; Cornil, J. Organic semiconductors: A theoretical characterization of the basic parameters governing charge transport. *Proc. Natl. Acad. Sci. U. S. A.* **2002**, *99*, 5804−5809.
(51) Valeev, E. F.; Coropceanu, V.; da Silva Filho, D. A.; Salman, S.; Brédas, J.-L. Effect of Electronic Polarization on Charge-Transport Parameters in Molecular Organic Semiconductors. *J. Am. Chem. Soc.* **2006**, *128*, 9882−9886.
(52) Löwdin, P. O. On the Non-Orthogonality Problem Connected with the Use of Atomic Wave Functions in the Theory of Molecules and Crystals. *J. Chem. Phys.* **1950**, *18*, 365−375.

DOI: 10.1021/acs.chemmater.9b01545
Chem. Mater. 2019, 31, 6424−6434

(53) Larsson, S. Electron transfer in chemical and biological systems. Orbital rules for nonadiabatic transfer. *J. Am. Chem. Soc.* **1981**, *103*, 4034−4040.
(54) Kobayashi, H. Sinusoidal structure of the 1:1 complex of phenothiazine and 7,7,8,8-tetracyanoquinodimethane, PTZ-TCNQ. *Acta Crystallogr., Sect. B: Struct. Crystallogr. Cryst. Chem.* **1974**, *30*, 1010−1017.
(55) Zhu, L.; Geng, H.; Yi, Y.; Wei, Z. Charge transport in organic donor-acceptor mixed-stack crystals: the role of nonlocal electron-phonon couplings. *Phys. Chem. Chem. Phys.* **2017**, *19*, 4418−4425.
(56) Karl, N.; Ketterer, W.; Stezowski, J. J. 1:1 donor-acceptor complex between phenazine and pyromellitic dianhydride at approx. 120 K. *Acta Crystallogr., Sect. B: Struct. Crystallogr. Cryst. Chem.* **1982**, *38*, 2917−2919.
(57) Munnoch, P. J.; Wright, J. D. Crystal structure of the 1:1 molecular complex of chrysene and 7,7,8,8-tetracyanoquinodimethane. *J. Chem. Soc., Perkin Trans. 2* **1974**, *2*, 1397−1400.
(58) Sato, R.; Kawamoto, T.; Mori, T. Asymmetrical hole/electron transport in donor-acceptor mixed-stack cocrystals. *J. Mater. Chem. C* **2019**, *7*, 567−577.
(59) Murphy, C. J.; Arkin, M.; Jenkins, Y.; Ghatlia, N.; Bossmann, S.; Turro, N.; Barton, J. Long-range photoinduced electron transfer through a DNA helix. *Science* **1993**, *262*, 1025−1029.
(60) Spoltore, D.; Hofacker, A.; Benduhn, J.; Ullbrich, S.; Nyman, M.; Zeika, O.; Schellhammer, S.; Fan, Y.; Ramirez, I.; Barlow, S.; Riede, M.; Marder, S. R.; Ortmann, F.; Vandewal, K. Hole Transport in Low-Donor-Content Organic Solar Cells. *J. Phys. Chem. Lett.* **2018**, *9*, 5496−5501.
(61) Melianas, A.; Pranculis, V.; Spoltore, D.; Benduhn, J.; Inganäs, O.; Gulbinas, V.; Vandewal, K.; Kemerink, M. Charge Transport in Pure and Mixed Phases in Organic Solar Cells. *Adv. Energy Mater.* **2017**, *7*, 1700888.
(62) Symalla, F.; Friederich, P.; Massé, A.; Meded, V.; Coehoorn, R.; Bobbert, P.; Wenzel, W. Charge Transport by Superexchange in Molecular Host-Guest Systems. *Phys. Rev. Lett.* **2016**, *117*, 276803.
(63) Han, G.; Yi, Y.; Shuai, Z. From Molecular Packing Structures to Electronic Processes: Theoretical Simulations for Organic Solar Cells. *Adv. Energy Mater.* **2018**, *8*, 1702743.

DOI: 10.1021/acs.chemmater.9b01545
Chem. Mater. 2019, 31, 6424−6434